Journal of Science and Technology in Civil Engineering, HUCE, 2026, 20 (3): 64–79

# PREDICTING COMPRESSIVE CREEP OF SCC BASED ON MODEL B4TW-SCC: OPTIMIZATION METHOD AND EXPERIMENTAL STUDY

Nguyen Doan Binh[a,*], Wen-Cheng Liao[b]

[a]*Faculty of Building Materials, Hanoi University of Civil Engineering, 55 Giai Phong road, Bach Mai ward, Hanoi, Vietnam*
[b]*Department of Civil Engineering, College of Engineering, National Taiwan University, Taipei, Taiwan*

***Article history:***
*Received 12/02/2026, Revised 27/5/2026, Accepted 12/6/2026, Available online 25/9/2026, Version of Record 25/9/2026*

**Abstract**

Many prediction models have been developed to address the disadvantages of creep, which is induced by a constant load on concrete structures, such as cracks, deflections, serviceability failures, and reduced long-term performance. However, the available models still lack accuracy in predicting the compressive creep of concrete, particularly in the case of self-compacting concrete (SCC), which differs from conventional concrete in its composition. Therefore, the model B4TW-SCC was calibrated using the B4 model to meet the SCC database requirements. The optimization of the new prediction model was carried out by evaluating statistical factors and the weighting plan, which subdivided the 266 test curves in the laboratory database into independent variables. The developed prediction model performed better than the other models, based on both the SCC database and experimental results in this study, which were conducted on the creep behaviour of SCC containing fly ash in different contents, 20% and 40% by mass of cementitious material.

*Keywords:* creep; database; model; self-compacting concrete; fly ash.

## 1. Introduction

The creep strain is influenced by various factors, such as the content of raw materials, relative humidity, stiffness, applied load, and specimen size [1]. Therefore, predicting creep is difficult and often requires considerable databases on experimental values. Preventing the cracking of concrete structures due to the impact of creep strain in civil engineering infrastructure is very important. Many prediction models have been developed to calculate the creep strain of conventional concrete [2–7]. However, the creep behaviour of plain concrete was significantly different from that of the self-compacting concrete (SCC), which has a higher powder content, lower aggregate volume, and smaller particle size of coarse aggregate [8–10].

In fact, the parameters are complicated and distributed in a large range with nonuniformity. Consequently, improper data can create biased statistical indicators and lead to an inefficient model [11]. Although several models have also been developed to calculate the creep of SCC, including the JSCE-SCC (Aslani) [12], CEB90-SCC (Poppe) [13], and CEB90-SCC (Kavanaugh) [14], these models were still inefficient in predicting the creep of SCC because the selected database was not relevant for the evaluation. Therefore, establishing a new prediction model appropriate for the complete SCC database is necessary.

*Corresponding author. *E-mail address:* binhnd@huce.edu.vn (Binh, N. D.)
https://doi.org/10.31814/stce.huce2026-20(3)-04 p-ISSN 1859-2996; e-ISSN 2734-9268
© 2026 The Author(s). Published by Hanoi University of Civil Engineering. Licensed under CC BY-NC-ND 4.0.

This paper introduced the optimization method for model B4TW-SCC, based on models B4 [7] and B4TW-2020 [15], developed to calculate the creep function of SCC. The new parameters would satisfy the assembled SCC database, comprising 266 test curves for both basic creep and total creep functions, which were observed on sealed and unsealed specimens, respectively. The optimum values were determined through a combination of statistical coefficients and proper data weighting. While acceptable statistical coefficients were used to minimize model error, the weighting scheme was based on the subdivision of independent variables to avoid biased evaluation. The efficiency of the model B4TW-SCC was compared with that of available prediction models, including the B4, the fib MC2010 [4], and other SCC models. Moreover, the creep behaviour of SCC with fly ash contents ranging from 20% to 40% by mass of cementitious materials was tested up to 252 days.

## 2. Experiment study

### *2.1. Materials and mix proportions*

The materials used to designate the mix proportions included cement (c), fly ash (FA), aggregate (a), superplasticizer (SP), and water (w). In which ordinary Portland cement and fly ash are combined to form the cementitious material (cm). The cement was of type I, as per the criteria of ASTM C150 [16], while the fly ash was of type F, based on ASTM C618 [17]. Sand (s) and coarse aggregate (ca) had maximum sizes of 5 mm and 12.5 mm, corresponding to water absorption rates of 1.29% and 0.77%, respectively [18, 19]. Additionally, the chemical admixture Master Glenium 8009-V2 played a primary role in reducing the high mixing water range and improving the workability of fresh concrete.

Table 1. Mix proportions and properties of SCC

| Mix | Materials by mass (kg/m$^3$) | | | FA/cm (%) | w/cm | SP (%) | Workability | | | $f_{cm28}$ (MPa) |
|---|---|---|---|---|---|---|---|---|---|---|
| | cm | s | ca | | | | Slump flow (mm) | $T_{50}$ (s) | V-funnel time (s) | |
| FA-20 | 496 | 853 | 853 | 20 | 0.36 | 0.88 | 710 | 5.7 | 18.3 | 53.6 |
| FA-40 | 490 | 842 | 842 | 40 | 0.36 | 0.94 | 710 | 5.6 | 18.2 | 50.3 |

Two mix proportions of SCC were designated as summarized in Table 1. In which FA-20 and FA-40 had fly ash with ratios of 20% and 40% by mass of cementitious material, respectively. The mix parameters were selected on the center point of the SCC database, which has the mean values including cm of approximate 500 kg/m$^3$, w/cm of 0.36, a/cm of 3.44, and s/a of 0.5. These values are also equal to the composition parameters of model B4TW-SCC.

### *2.2. Experimental procedure*

The trial batches of mix proportions were blended in a two-shaft machine with a high engine power of approximately 5.6 kW for a total of 8 minutes. Thereafter, the fresh condition of SCC was evaluated using the slump flow, $T_{50}$ time (according to ASTM C1611 [20]), and V-funnel flow time, as guidance from EN 12350-9 [21]. All the specimens were moulded without any vibration and immediately covered the top surface to prevent moisture loss. After 24 hours, the specimens were demoulded and cured in a moist condition at a temperature of 23 ± 2 °C and a relative humidity of over 95%. At the age of 28 days, the shrinkage and creep specimens were transferred to the drying room (temperature of 23 ± 2 °C and relative humidity of 50 ± 4%). The shrinkage strain was measured by length comparator following ASTM C157 [22], with a 75 × 75 × 285-mm prism specimen for autogenous shrinkage and a 75 × 75 × 285-mm prism for total shrinkage. The creep strain was tested

on 100 mm × 200 mm cylindrical specimens according to ASTM C512 [23]. The specimens of autogenous shrinkage and basic creep were sealed with different layers of plastic sheets and aluminium foil. Additionally, the total shrinkage and total creep were tested on unsealed specimens. The constant stress applied to the creep specimens was 30% of the 28-day compressive strength, which was determined on cylindrical specimens measuring 100 mm × 200 mm, as per the guidelines of ASTM C39 [24]. For the preparation of the creep experiment, two pairs of pre-drilled brass discs were fixed 200 mm apart, which was considered the initial length, using AB-epoxy glue on both sides along the lateral axis of the specimens. The next deformation values were measured by the demountable mechanical strain gauge equipment. In each loading frame, three specimens were linked together by high-strength gypsum, as illustrated in Fig. 1.



(a) Sealed specimens (b) Unsealed specimens

Figure 1. Set up of the creep experiment

## 3. Experiment results

### *3.1. Workability and compressive strength*

The workability of fresh SCC met the requirements of European guidelines [25]. As shown in Table 1, the slump flow was achieved at 710 mm without segregation by visual assessment, while the $T_{50}$ time of the concrete was nearly 6 seconds. This value demonstrates the spread capacity of SCC containing fly ash, which has a ball-bearing effect due to the tiny spherical particles, as studied by Lee et al. [26]. The enhancement of fly ash on the workability of SCC has also been reported by other authors [27, 28]. However, when the amount of fly ash increased from 20% to 40%, the compressive strength decreased slightly by about 6% at the 28-day testing age. The impact of fly ash on mechanical properties was also investigated by Mustapha et al. [29] and Pham [30]. In this studies, the researchers explained that fly ash reduces the early-age strength of concrete because the pozzolanic reaction occurs slowly at the initial stage of hydration, particularly when a high volume of fly ash was used to replaced partially cement content.

### *3.2. Creep behaviour*

The creep function (or compliance function) can be calculated through the elastic strain and creep strain under the constant applied stress as follows:

$$J(t, t_0) = \frac{\varepsilon_e(t_0) + \varepsilon_{cc}(t, t_0)}{\sigma(t_0)} \quad (1)$$

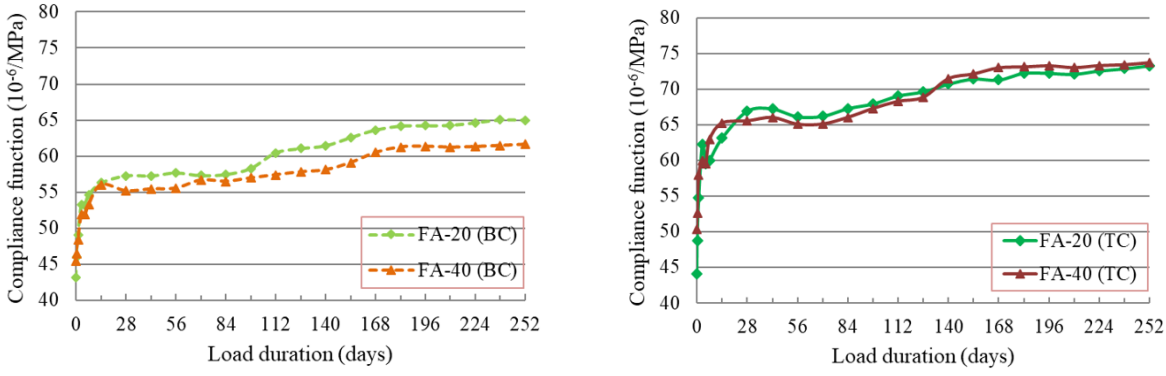
where $J(t, t_0)$ is the creep function ($10^{-6}$/MPa); $\varepsilon_e(t_0)$ is the elastic strain at loading age ($10^{-6}$ m/m); $\varepsilon_{cc}(t_0)$ is the creep strain ($10^{-6}$ m/m); $\sigma(t_0)$ is the applied stress (MPa); $t_0$ is loading age (days); $t$ is current age (days).

The creep strain can be calculated as

$$\varepsilon_{cc}(t, t_0) = \varepsilon(t, t_0) - \varepsilon_e(t_0) - \varepsilon_{cs}(t, t_c) \quad (2)$$

where $\varepsilon(t, t_0)$ is total strain ($10^{-6}$ m/m); $\varepsilon_{cs}(t, t_c)$ is the shrinkage strain ($10^{-6}$ m/m); $\varepsilon_e(t_0)$ is elastic strain ($10^{-6}$ m/m).

The final results of the basic creep (BC) function and the total creep (TC) function based on experimental data were presented in Fig. 2. It is clearly seen that the creep function decreases with an increase in fly ash content, particularly in sealed specimens. The basic creep function of mix FA-40 was nearly 5% than that of mix FA-20 at loading age of 252 days, while the total creep function was quite similar in varied content of fly ash from 20% to 40%. The detailed results of the creep behaviour of SCC at 252 days after loading are summarized in Table 2. It is clearly seen that the creep values are influenced directly by the applied stress on the specimens, as presented by Neville et al. [31]. Moreover, the delayed pozzolanic reactions of fly ash also could enhance the long-term compressive strength of concrete, particularly high amount of mineral admixture [32, 33], which relates inversely to the later magnitude of creep.




(a) Basic creep (b) Total creep

Figure 2. Compliance function of SCC

Table 2. The creep results of specimens

| Mix | $f_{cm28}$ (MPa) | $\sigma/f_{cm28}$ | $\sigma$ (MPa) | $\varepsilon_e$ ($10^{-6}$) | Creep results at 252 days after loading | | | |
|---|---|---|---|---|---|---|---|---|
| | | | | | $\varepsilon$ ($10^{-6}$) | $\varepsilon_{cs}$ ($10^{-6}$) | $\varepsilon_{cc}$ ($10^{-6}$) | $J$ ($10^{-6}$/MPa) |
| FA-20 (BC) | 53.6 | 0.3 | 16.3 | 704 | 1202 | 143 | 356 | 65.0 |
| FA-40 (BC) | 50.3 | 0.3 | 15.3 | 694 | 1105 | 164 | 248 | 61.6 |
| FA-20 (TC) | 53.6 | 0.3 | 16.3 | 718 | 1828 | 634 | 477 | 73.3 |
| FA-40 (TC) | 50.3 | 0.3 | 15.3 | 768 | 1724 | 598 | 358 | 73.7 |

## 4. Optimization of model B4TW-SCC for creep

### *4.1. Main formulae of model B4TW-SCC for creep*

The formulae of the model B4TW-SCC were adjusted to the mean values of composition, which include w/cm of 0.36, a/cm of 3.4, cm of 506 kg/m$^3$ corresponding to 4.6 standardized by the concrete

density ($\rho$ = 2350 kg/m$^3$), and ca of 840 kg/m$^3$ based on the SCC database, compared to the model B4 and model B4TW-2020. The total compliance function is given as

$$J(\hat{t},\hat{t}_0) = q_1 + C_b(\hat{t},\hat{t}_0) + C_d(\hat{t},\hat{t}_0,\tilde{t}_c) \tag{3}$$

where $\hat{t}$ is temperature-adjusted current age (days); $\hat{t}_0$ is temperature-adjusted age at loading (days); $\tilde{t}_c$ is temperature-adjusted age at exposure (days); $C_b(\hat{t},\hat{t}_0)$ is basic creep compliance ($10^{-6}$/MPa); $C_d(\hat{t},\hat{t}_0,\tilde{t}_c)$ is drying creep compliance ($10^{-6}$/MPa).

The instantaneous compliance is expressed as follows:

$$q_1 = \frac{p_1}{E_{cmt_0}} \tag{4}$$

Basic creep compliance is calculated by

$$C_b(\hat{t},\hat{t}_0) = q_2 Q(\hat{t},\hat{t}_0) + q_3 \ln\left[1 + (\hat{t}-\hat{t}_0)^{0.1}\right] + q_4 \ln\left(\frac{\hat{t}}{\hat{t}_0}\right) \tag{5}$$

The aging viscoelastic creep $q_2$ can be expressed as

$$q_2 = \frac{\alpha_2 p_2}{1\ GPa}\left(\frac{w/cm}{0.36}\right)^{p_{2w}}\left(\frac{4.6cm}{\rho}\right)^{p_{2c}}\left(\frac{ca}{840}\right)^{p_{2ca}} \tag{6}$$

The nonaging viscoelastic creep $q_3$ is given as

$$q_3 = \alpha_3 p_3 q_2\left(\frac{a/cm}{3.4}\right)^{p_{3a}}\left(\frac{w/cm}{0.36}\right)^{p_{3w}} \tag{7}$$

The flow compliance $q_4$ can be expressed as

$$q_4 = \frac{\alpha_4 p_4}{1\ GPa}\left(\frac{a/cm}{3.4}\right)^{p_{4a}}\left(\frac{w/cm}{0.36}\right)^{p_{4w}} \tag{8}$$

The drying creep compliance is given as follows.

$$C_d(\hat{t},\hat{t}_0,\tilde{t}_c) = q_5\{\exp[-p_{5H}H(\hat{t},\tilde{t}_c)] - \exp[-p_{5H}H_c(\hat{t}'_c,\tilde{t}_c)]\}^{0.5} \tag{9}$$

The drying creep $q_5$ as presented in the following equation

$$q_5 = \frac{\alpha_5 p_5}{1\ GPa}\left(\frac{a/cm}{3.4}\right)^{p_{5a}}\left(\frac{w/cm}{0.36}\right)^{p_{5w}}\left|k_h \varepsilon_{shu}(\tilde{t}_c)\right|^{p_{5\varepsilon}} \tag{10}$$

where $E_{cmt0}$ is modulus of elasticity at loading age $t_0$ (MPa); $\rho$ is unit weight of concrete (kg/m$^3$); $H(\hat{t},\tilde{t}_c)$, $H_c(\hat{t}'_c,\tilde{t}_c)$ are the spatial averages of pore relative humidity. The last formulae of the model B4TW-SCC for creep remained as given in the model B4 [7]. The values of creep parameters in Eqs. (4) and (6)–(10) are summarized in Tables 3 and 4, while the correction factors for admixture $\alpha_2$, $\alpha_3$, $\alpha_4$, $\alpha_5$ are shown in Table 5. The humidity-dependent factor $k_h$ and ultimate drying shrinkage strain $\varepsilon_{shu}(\tilde{t}_c)$, the formulae of these factors are the same as given in model B4TW-SCC for shrinkage of SCC [34].

Table 3. Creep parameters of the model B4TW-SCC for creep

| Cement | $p_1$ | $p_2$ | $p_3$ | $p_4$ | $p_5$ | $p_{5H}$ |
|---|---|---|---|---|---|---|
| Normal type (R) | 1.3 | $50 \times 10^{-3}$ | $40 \times 10^{-3}$ | $4 \times 10^{-3}$ | $700 \times 10^{-6}$ | 7 |

Table 4. Creep exponents of the model B4TW-SCC for creep

| Cement | $p_{2w}$ | $p_{2c}$ | $p_{2ca}$ | $p_{3a}$ | $p_{3w}$ | $p_{4a}$ | $p_{4w}$ | $p_{5\varepsilon}$ | $p_{5a}$ | $p_{5w}$ |
|---|---|---|---|---|---|---|---|---|---|---|
| Normal type (R) | 2.0 | 1.1 | 0.2 | −0.8 | 0.3 | −0.7 | 2.58 | −0.76 | −0.5 | 4.0 |

Table 5. Scaling parameters of the model B4TW-SCC for creep

| Admixture class (% of cm) | $\alpha_2$ | $\alpha_3$ | $\alpha_4$ | $\alpha_5$ |
|---|---|---|---|---|
| Slag | 1.0 | 1.0 | 1.3 | 0.9 |
| Fly ash | 1.0 | 1.0 | 1.4 | 0.9 |
| Slag and fly ash | 1.2 | 1.0 | 3.5 | 1.2 |
| Silica fume | 1.0 | 1.0 | 1.4 | 0.9 |

### *4.2. Optimization method*

Two key statistical coefficients were used to assess the creep prediction model, including the determination coefficient $R^2$ [35, 36] and the normalized root mean square error (*NRMSE*) [37, 38]. The errors of the prediction model were minimized using $R^2$ and *NRMSE*, and a screening assessment was conducted to determine the optimal efficiency based on the distribution of experimental data points and predicted values in the diagram. However, if the optimization was carried out only on these coefficients, the model would still be subject to biased evaluation because a large portion of them has a significant impact on the statistical results. In the laboratory database, the number portion of data sets tends towards the short loading duration, small testing sizes, and early loading ages. Therefore, it is necessary to evaluate the model on both acceptable statistical indicators and a weighting scheme to attain the preferred model [39, 40]. The subdivisions of independent variables were divided into the appropriate data sets, including loading duration $(t - t_0)$, environmental humidity ($RH$), specimen size ($V/S$), and loading age $t_0$ [11]. According to the database, which contains 54 test curves of basic creep and 212 test curves of total creep, representing approximately 22% and 78% of the total data, respectively. The data are divided into subsets based on a proper number, as listed in Tables 6 and 7, respectively. Among the different types of cement, only the normal type (R) had the largest number of data sets up to 68% in the creep database, while the other cement types only included approximately 16% slow hardening cement (SL) and 16% rapid hardening cement (RS). Therefore, the cement type R was chosen to calibrate the prediction model during the optimization process. This issue was also the applicable limit of this study. However, the calibrating strategy of type R can be used for the last cement types in case of an adequate database.

Based on the database subsets, the parameters of model B4TW-SCC were determined using an optimal procedure, carried out sequentially from the most to least important parameters. In which the parameters related to w/cm were considered the most important, while the parameters associated with a/cm were found to be the second most important [40].

The three-step optimum process was applied to model B4TW-SCC for compressive creep, as illustrated in Fig. 3. Firstly, the instantaneous compliance was initially calibrated, and the evaluation of the prediction formulae on static elastic modulus was also considered into calculation. In the next

step, the parameters of basic creep compliance were determined on 10 values for SCC using only Portland cement and 12 values for the concrete containing mineral admixtures. The last step ascertained the drying creep compliance parameters based on the interaction with the creep compliance function in the SCC database, resulting in a total of nine new values. The parameters were developed to improve the accuracy of the prediction model B4TW-SCC for the creep of SCC.

Table 6. Independent variables of the database for basic creep

| $t - t_0$ (days) | | $t_0$ (days) | |
|---|---|---|---|
| Scope | Datasets | Scope | Datasets |
| ≤ 90 | 23 | ≤ 7 | 21 |
| 90–210 | 12 | 7–28 | 29 |
| 210–655 | 19 | 28–105 | 4 |

Table 7. Independent variables of the database for total creep

| $t - t_0$ (days) | | *V/S* (mm) | | *RH* (%) | | $t_0$ (days) | |
|---|---|---|---|---|---|---|---|
| Scope | Datasets | Scope | Datasets | Scope | Datasets | Scope | Datasets |
| ≤ 90 | 59 | 15–22 | 66 | 35–50 | 117 | ≤ 7 | 77 |
| 90–210 | 65 | 22–26 | 71 | 50–60 | 80 | 7–28 | 123 |
| 210–655 | 88 | 26–41 | 75 | 60–85 | 15 | 28–105 | 12 |

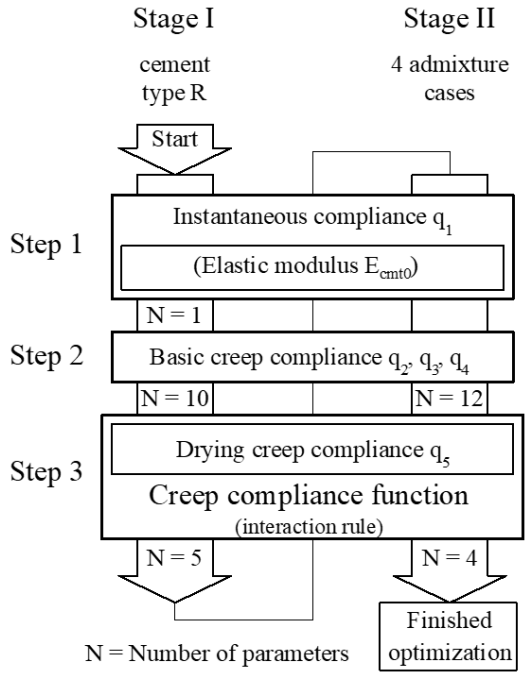



Figure 3. Optimum process of model B4TW-SCC for compressive creep

### *4.3. Optimization parameters of instantaneous compliance*

Firstly, the equation for the static elastic modulus was evaluated among different prediction formulae for conventional concrete. Moreover, the components of SCC could also affect the modulus

of elasticity. Therefore, the prediction formulae for compressive strength and modulus of elasticity should be evaluated initially before proceeding with the other steps of the optimization for the creep function. In this study, a database of static modulus of elasticity for SCC containing natural aggregate, based on cylinder compressive strength, has been compiled from 264 published papers, totaling 1546 data points. This database was divided into different subsets based on the loading age ($t_0$), with proper numbers of data points, including 401 ($t_0 < 28$ days), 772 ($t_0 = 28$ days), and 373 ($t_0 > 28$ days). As shown in Fig. 4, the coefficient of elastic modulus for SCC with normal Portland cement (type R) was optimized to a value of 4734 based on testing age, which is compatible with the equation of the model B4 and the model ACI 209R-92. Therefore, the prediction formulae of elastic modulus were suggested as follows.

$$E_{cmt_0} = 4734\sqrt{f_{cmt_0}} \tag{11}$$

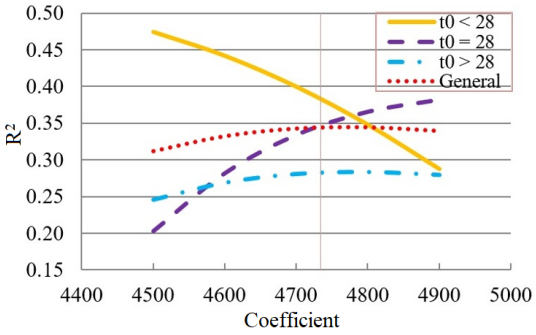



Figure 4. Optimization of elastic modulus

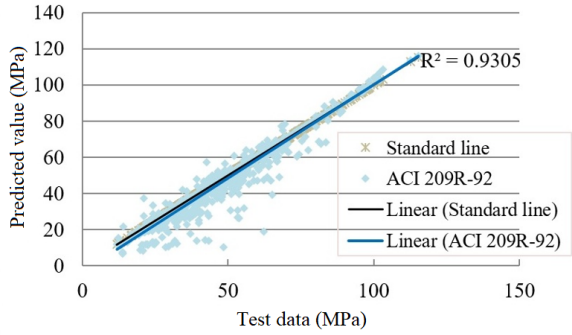


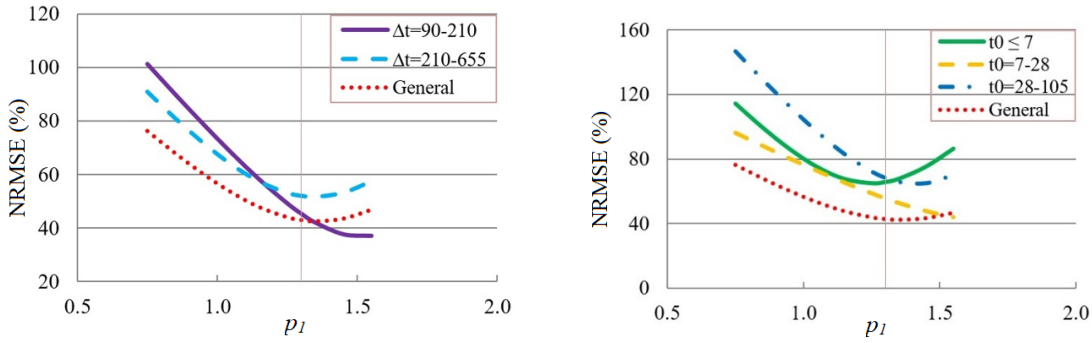

Figure 5. Prediction of compressive strength

According to the strength database, which was assembled over 1100 data points of SCC using the normal cement type, the compressive strength formulae based on the model ACI 209R-92 demonstrated efficiency in predicting the SCC strength at different ages, as illustrated in Fig. 5. The value $R^2$ was 0.93, which exhibited closely calculated values compared to the experimental data. Moreover, most data points were scattered uniformly along the standard line in the diagram. Therefore, the prediction formulae for compressive strength at the loading age can be calculated using the 28-day value, as per the model ACI 209R-92. The equation for predicting the compressive strength of SCC using cement type R is expressed as

$$f_{cmt0} = \left(\frac{t_0}{4 + 0.85 \cdot t_0}\right) f_{cm28} \tag{12}$$

where $f_{cmt0}$ is $t_0$-day compressive strength (MPa); $f_{cm28}$ is 28-day compressive strength (MPa).

The study affirmed that the formulae of model B4 and model ACI 209R-92 could be satisfy absolutely the SCC database in calculating the elastic modulus and compressive strength at different loading ages based on the value of 28-day compressive strength. Therefore, the results also present an important contribution in developing the model B4TW-SCC. After the prediction formulae for the elastic modulus and compressive strength were calibrated, the parameter $p_1$ of instantaneous compliance was determined using the independent variables from the exterior factors of the basic creep database. The reason for using sealed specimens was that they had fewer influential factors and higher reliability than unsealed specimens, which were affected by drying conditions. As shown in Fig. 6, the optimum value of parameter $p_1$ was found at 1.3.



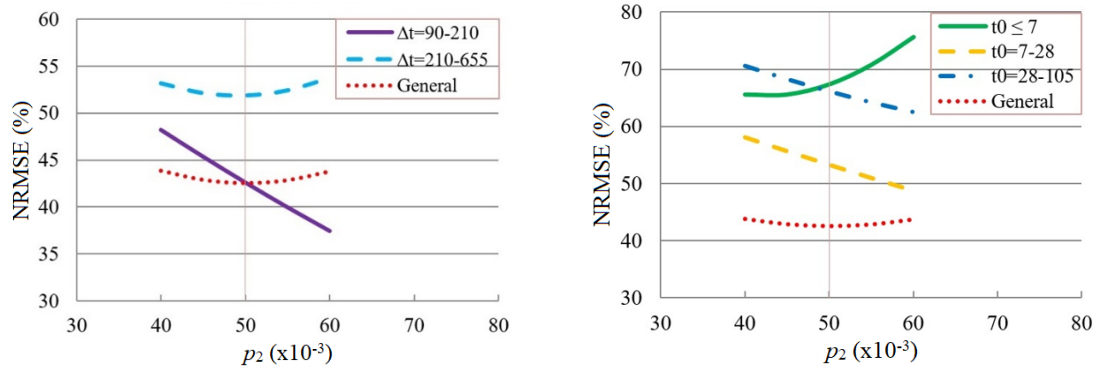

(a) Load duration (b) Loading age

Figure 6. Optimization of parameter $p_1$ of the model B4TW-SCC

### *4.4. Optimization parameters of SCC without mineral admixture*

a. Basic creep compliance

The optimization of basic creep compliance was carried out in order as $p_2$, $p_3$, $p_4$, $p_{2w}$, $p_{2c}$, $p_{2ca}$, $p_{3w}$, $p_{3c}$, $p_{4w}$, and $p_{4a}$ based on important roles of parameters. This order is also the careful investigated result of the parameters on the creep predictability. Firstly, based on the subsets of the variables, involving load duration and loading age (Table 6), the parameter $q_2$ was optimized to a value of $50 \times 10^{-3}$, as illustrated in Fig. 7. The value should be selected based on the minimum acceptable errors for balancing all subsets of the independent variables. Then, the other parameters of basic creep were evaluated similarly to parameter $q_2$, and the final results are presented in Tables 3 and 4.



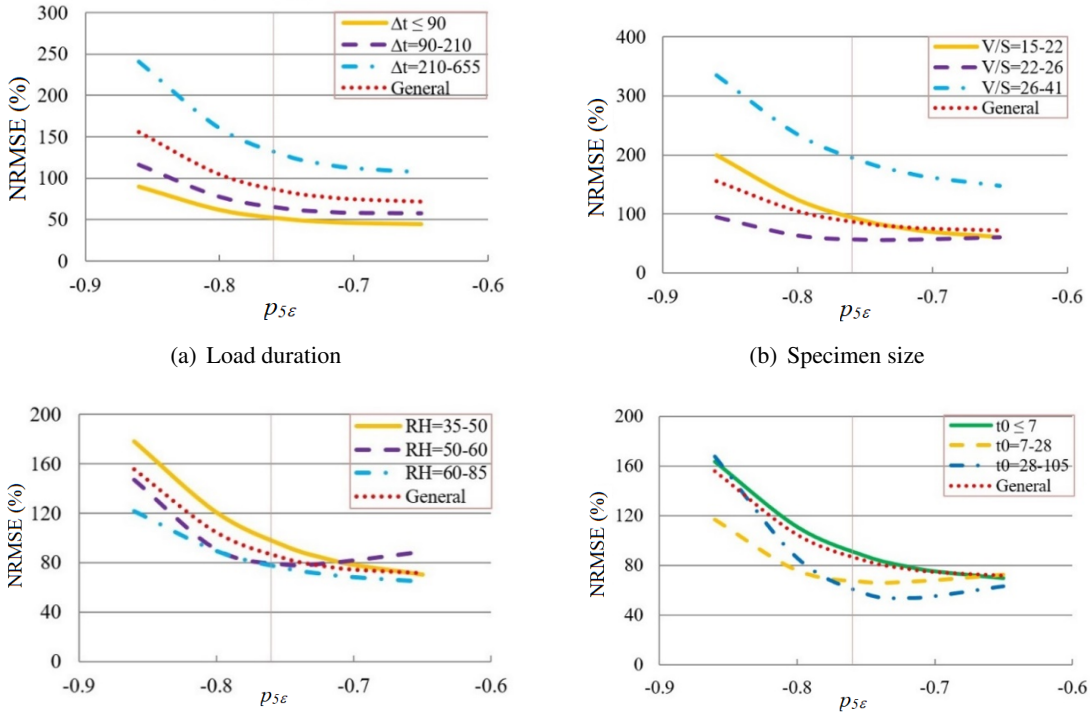

(a) Load duration (b) Loading age

Figure 7. Optimization of parameter $p_2$ of the model B4TW-SCC

b. Drying creep compliance

The optimization procedure for drying creep was carried out similarly to that for basic creep. However, unsealed specimens were affected by loss of moisture during the drying condition, so that the process should be considered with more independent variables than basic creep, including load duration, specimen size, relative humidity, and loading age, as shown in Table 7. Based on the independent variables, parameters of drying creep depending on cement type were determined in the following sequence: $p_{5\varepsilon}$, $p_{5w}$, $p_{5a}$, $p_5$, and $p_{5H}$. Consequently, this clear optimum order also

indicated the novelty of this study compared to the calibration of the ordinary model B4. Initially, the parameter $p_{5\varepsilon}$ was optimized to −0.76, which was expected to satisfy all acceptable error bounds for the subsets, as shown in Fig. 8. The results show that the parameter $p_{5\varepsilon}$ significantly affects the magnitude of drying creep. Similarly, the last parameters of drying creep were investigated as parameter $p_{5\varepsilon}$, and their optimum values are listed in Tables 3 and 4.




(a) Load duration

(b) Specimen size

(c) Relative humidity

(d) Loading age

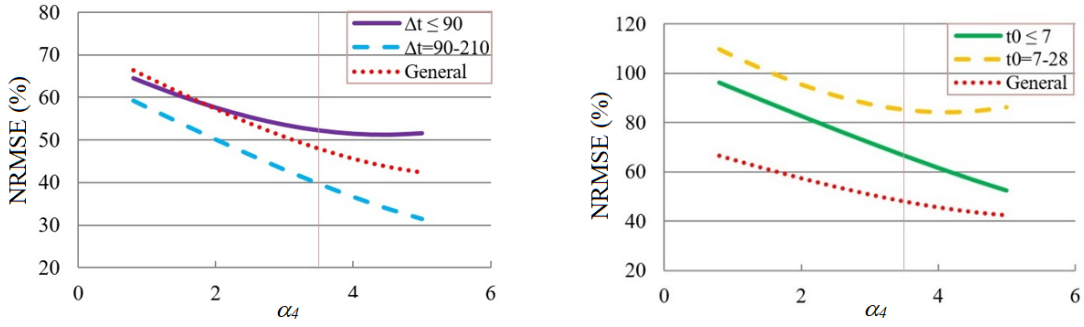
Figure 8. Optimization of parameter $p_{5\varepsilon}$ of the model B4TW-SCC

### *4.5. Optimization parameters of SCC using mineral admixtures*

After optimizing the creep parameters for SCC without mineral admixtures based on ordinary Portland cement, scaling parameters were introduced to improve the predicted accuracy of concrete containing mineral admixtures. In the creep database, SCC used mostly slag, fly ash, and silica fume as supplementary cementitious materials. In which the data sets of SCC incorporating slag, fly ash, a combination of slag and fly ash, and silica fume get to 12%, 21%, 20%, and 5%, respectively. The scaling factors also demonstrated the significant influence of admixture on the time-dependent deformation of SCC. The parameters start at their original values of 1. Then their new values are optimized by combining the evaluation of statistical coefficients with a weighting scheme, similar to the process of SCC without mineral admixtures.

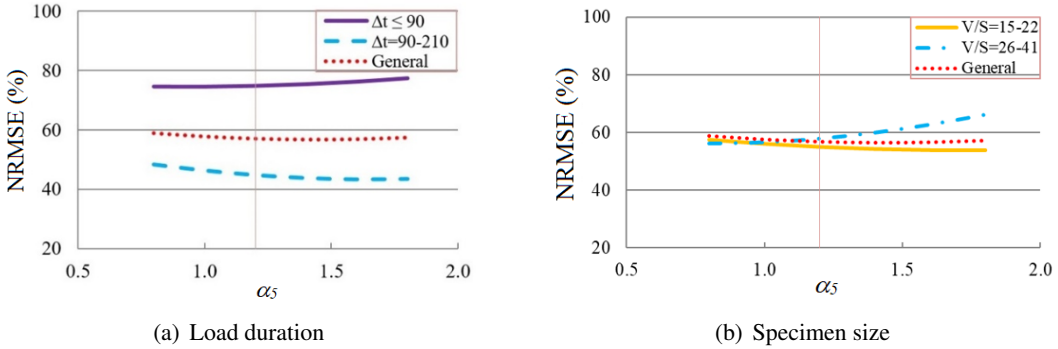
The optimization procedure for scaling factors of SCC containing the combination of slag and fly ash yielded results as illustrated in Figs. 9 and 10. The parameter $\alpha_4$ for basic creep was optimized to 3.5 based on subsets of load duration and loading age, as shown in Fig. 9. Additionally, the parameter $\alpha_5$ of drying creep was selected to achieve an acceptable result of 1.2, which satisfied all independent variables, including loading duration, specimen size, relative humidity, and loading age, as shown in Fig. 10. The last scaling parameters of SCC were likely optimized with respect to the factors $\alpha_4$ and

$\alpha_5$. The final results of all adjusted factors were presented in Table 5. The calibration of model B4TW-SCC for mineral admixtures also differed significantly from that of model B4, which optimized the scaling factors for chemical additives commonly used in the composition of conventional concrete. However, the prediction capacity of model B4TW-SCC was the least accurate for SCC containing fly ash among the mineral admixtures used in the creep database, particularly for the amount of fly ash replacing cement content by weight under 40%. These predicted results could be impacted by the large difference in chemical composition of the fly ash, including type F and type C, as the criteria of ASTM C618-22 [17]. Therefore, further study of the creep of concrete using fly ash requires additional investigation.

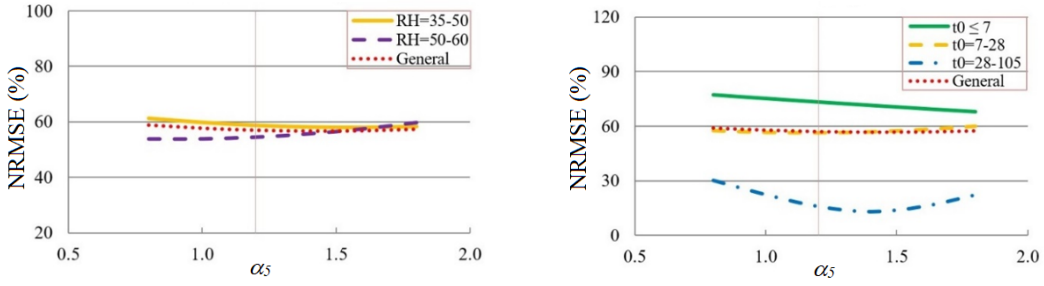



(a) Load duration (b) Loading age

Figure 9. Optimum parameter $\alpha_4$ for basic creep of SCC using slag and fly ash




(a) Load duration (b) Specimen size



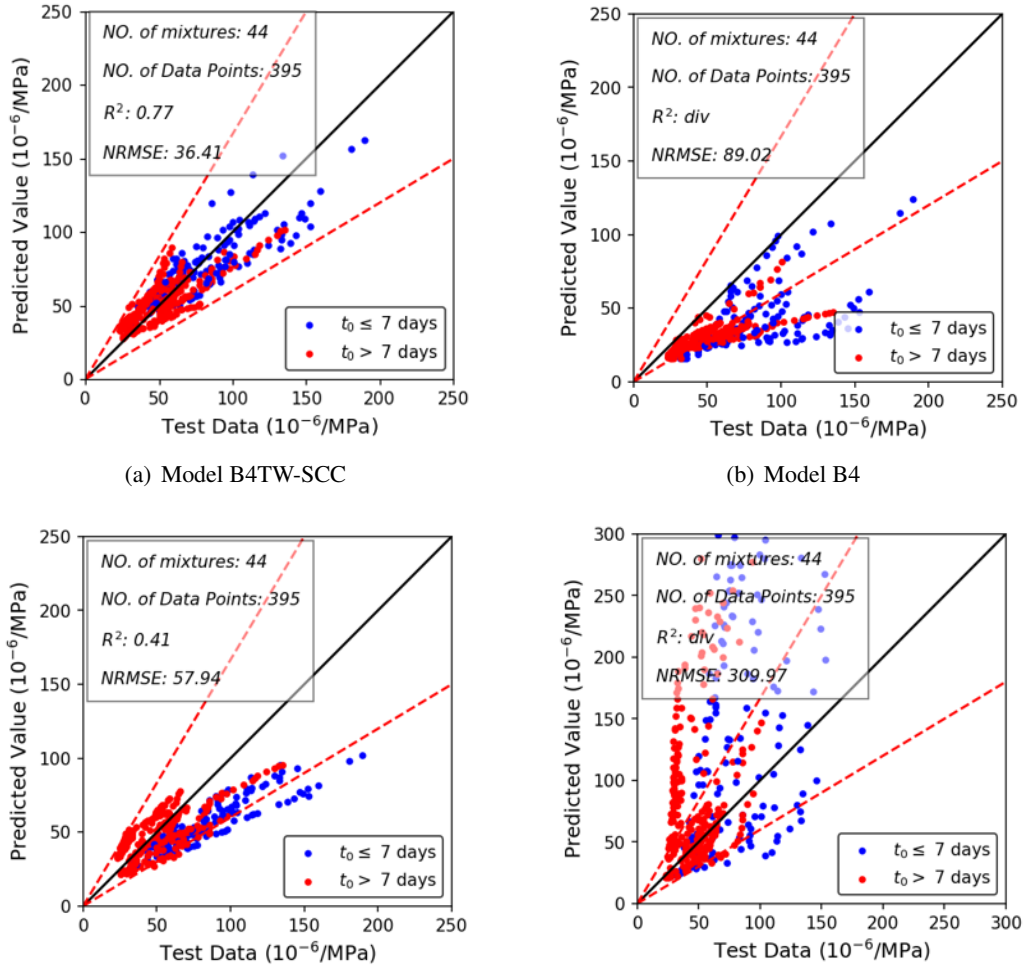

(c) Relative humidity (d) Loading age

Figure 10. Optimum parameter $\alpha_5$ for drying creep of SCC using slag and fly ash

## 5. Evaluation of prediction models on creep data

### *5.1. Evaluation of models on the creep database*

The assessment of prediction models based on the SCC database for basic creep is presented in Fig. 11. In which the data points of the model B4TW-SCC were distributed uniformly within the acceptable error of ±40% in the diagram. This prediction model showed the highest accuracy in predicting the basic creep function, with an *NRMSE* of 36%, while model B4 had an *NRMSE* of 89%. Moreover, the model fib MC2010 also underestimated the creep data, with most data points towards the x-axis. Particularly, the JSCE-SCC (Aslani) model overestimated the basic creep of SCC, with an *NRMSE* exceeding 309%, which is considered as the maximum error among the prediction models.




(a) Model B4TW-SCC

(b) Model B4

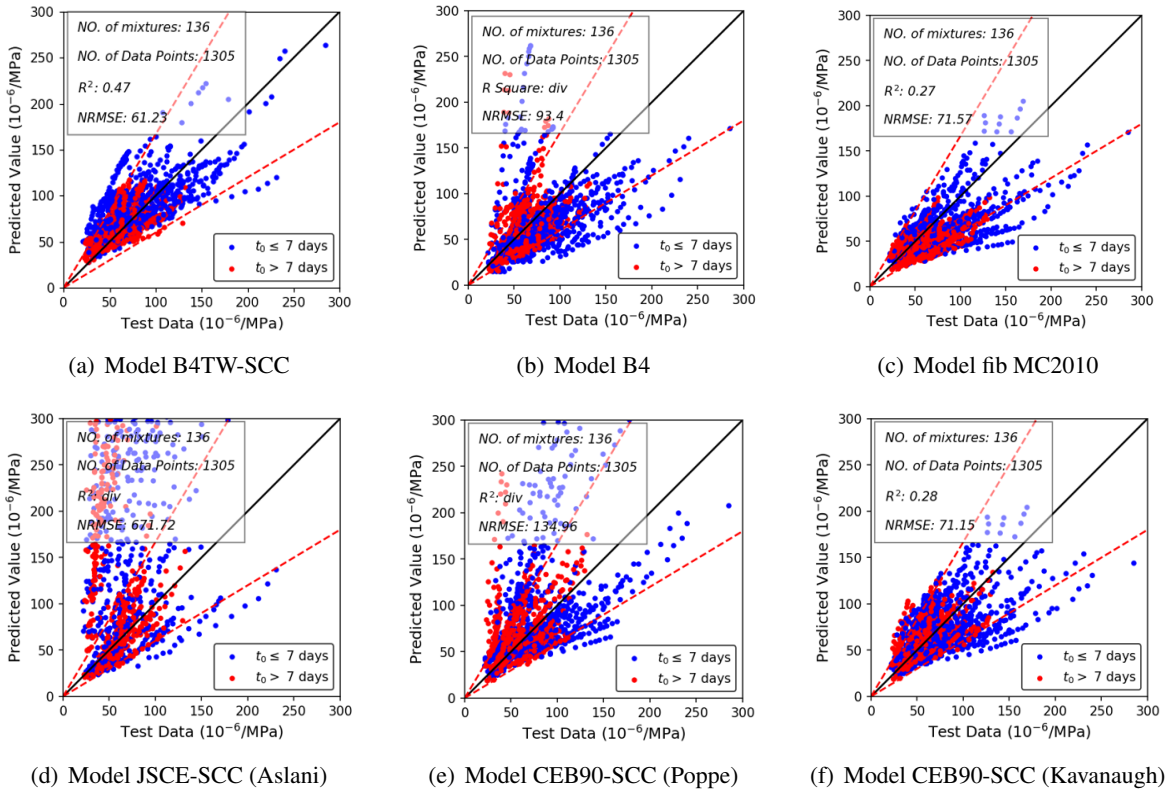
(c) Model fib MC2010

(d) Model JSCE-SCC (Aslani)

Figure 11. Evaluation of prediction models on the basic creep function

The model B4TW-SCC also accurately predicted the total creep function of SCC, as illustrated in Fig. 12. This model exhibited the lowest error, with a determination coefficient $R^2$ of 0.47 and an *NRMSE* of 61%. Additionally, the distribution of the 1305 data points was well-scattered within the acceptable range of ±40%. On the other hand, the predicted values from the original model B4 were widely separated, with an *NRMSE* of up to 93%. The last models also exhibited high errors,

with *NRMSE* values of approximately 672%, 135%, and 71% for the models JSCE-SCC (Aslani), CEB90-SCC (Poppe), and CEB90-SCC (Kavanaugh), respectively.




(a) Model B4TW-SCC (b) Model B4 (c) Model fib MC2010

(d) Model JSCE-SCC (Aslani) (e) Model CEB90-SCC (Poppe) (f) Model CEB90-SCC (Kavanaugh)

Figure 12. Evaluation of prediction models on the total creep function

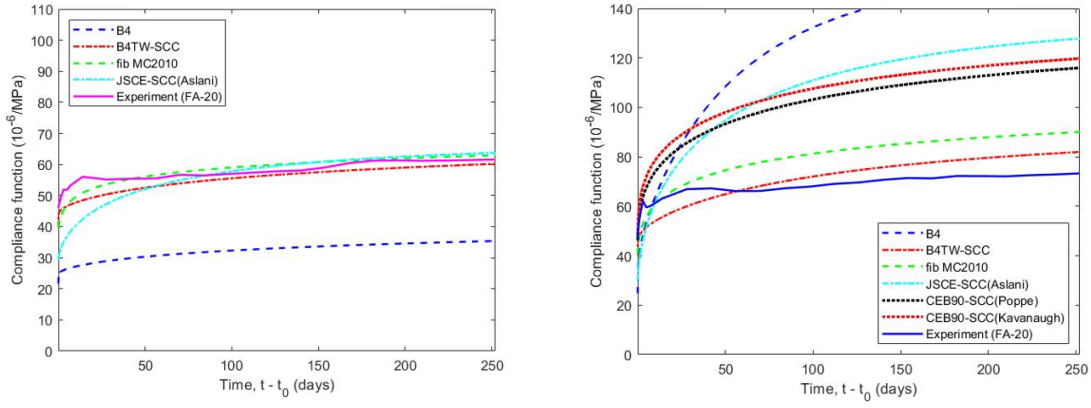
### *5.2. Evaluation of models on test results*

As shown in Fig. 13(a) and Fig. 14(a), the estimated values of model B4TW-SCC were close to the basic creep function of SCC containing fly ash in the range of 20% to 40% during the load stage up to 252 days. The results indicated a significant improvement in the prediction model based on the optimum parameters compared to the original model B4, which yielded the lowest value among the prediction models. Moreover, the fib MC2010 also accurately predicted the experimental data, with predicted values slightly higher, ranging from 4% to 6%, than those of model B4TW-SCC at the last loading age. The other model, JSCE-SCC (Aslani), was inconsistent with the tested basic creep function at the early-age stage and reached the predicted value of the model fib MC2010 at the later loading age.

The model B4TW-SCC also performed well in the experimental total creep of SCC containing fly ash, as shown in Fig. 13(b) and Fig. 14(b). The error of this improved model was the lowest, at approximately 12% at a loading age of 252 days, compared to the other models. Even the error of model fib MC2010 is also higher than that of model B4TW-SCC, at 10% for mix FA-20 and 15% for mix FA-40. The other models overestimated the total creep function, with errors of at least 58%, particularly model B4 for mix FA-20 and model JSCE-SCC (Aslani) for mix FA-40.

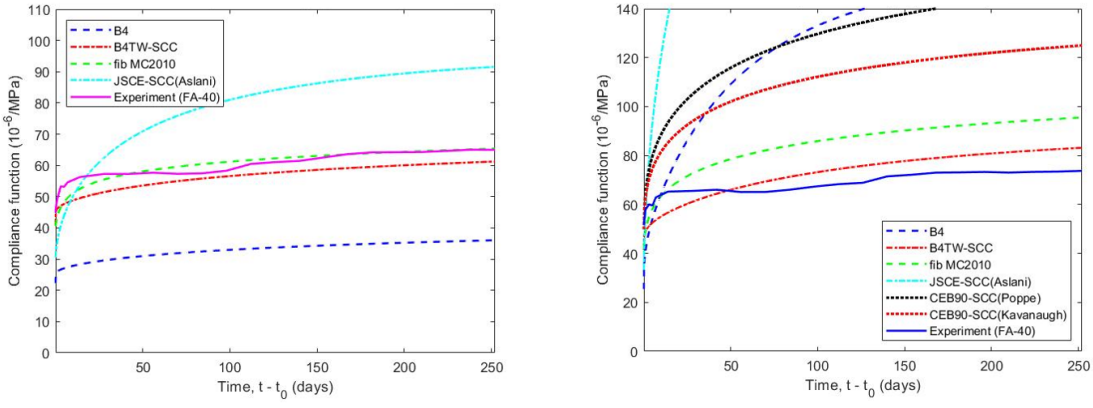
According to the formulae of model B4TW-SCC, the instantaneous compliance was related negatively to the applied stress. Consequently, when the applied stress of mix FA-40 was decreased

approximately 6% compared to that of mix FA-20, as the experiment results, the predicted values of basic creep function and total creep function were increased negligibly by about 2% and 1.6% at 252 days after loading age, respectively.




(a) Basic creep (b) Total creep

Figure 13. Evaluation of prediction models on the creep function of mix FA-20




(a) Basic creep (b) Total creep

Figure 14. Evaluation of prediction models on the creep function of mix FA-40

## 6. Conclusions

According to the optimization process of the model B4TW-SCC in predicting compressive creep of SCC containing normal cement type, the main conclusions can be drawn as follows:

(1) The model B4TW-SCC was calibrated on model B4 to satisfy the SCC database, comprising 54 test curves of basic creep and 212 test curves of total creep. The formulae for model B4TW-SCC were adjusted using new mean values from the SCC database. Moreover, the total number of parameters was optimized up to 32 values based on the statistical coefficients and the weighting plan.

(2) The total and basic creep functions of SCC were significantly influenced by fly ash content in the range of 20% to 40% as a partial replacement for cement and by experimental conditions.

(3) The model B4TW-SCC exhibited the highest efficiency in estimating both the basic and total creep functions of SCC among the available prediction models. However, the accuracy of the predic-

tion model B4TW-SCC, which was influenced significantly with the number of collected test curves, could still be improved by updating the SCC database in further work.

## Declaration of generative AI and AI-assisted technologies

The author(s) declare that no generative AI or AI-assisted technologies were used in the preparation of this manuscript.

## References


[1] Bažant, Z. P. (1988). *Mathematical modelling of creep and shrinkage of concrete*. John Wiley & Sons, New York.

[2] ACI 209R-92 (1992). *Prediction of creep, shrinkage, and temperature effects in concrete structures*. Farmington Hills, MI: American Concrete Institute.

[3] CEB (1991). *CEB-FIP model code 1990 (MC90)*. Geneva: Comité Euro-International du Béton.

[4] fib MC2010 (2013). *fib model code for concrete structures 2010*. Geneva: International Federation for Structural Concrete.

[5] AASHTO (2017). *AASHTO LRFD bridge design specifications*. Washington, DC: American Association of State Highway and Transportation Officials.

[6] JSCE (2007). *Standard specifications for concrete structures 'Design'*. Tokyo: Japan Society of Civil Engineers.

[7] Bažant, Z. P., Wan-Wendner, R. (2015). Model B4 for creep, drying shrinkage and autogenous shrinkage of normal and high-strength concretes with multi-decade applicability. *Materials and Structures*, 48: 753–770.

[8] ACI 237R-07 (2007). *Self-consolidating concrete*. Farmington Hills, MI: American Concrete Institute.

[9] Leemann, A., Lura, P., Loser, R. (2011). Shrinkage and creep of SCC: The influence of paste volume and binder composition. *Construction and Building Materials*, 25(5):2283–2289.

[10] Lowke, D., Schießl, P. (2009). Effect of powder content and viscosity agents on creep and shrinkage of self-compacting concrete. In *CONCREEP 8*, Ise-Shima, Japan, 655–661.

[11] Bažant, Z. P., Li, G. H. (2007). *Unbiased statistical comparison of creep and shrinkage prediction models*. Technical report, Evanston, Illinois.

[12] Aslani, F., Nejadi, S. (2013). Creep and shrinkage of self-compacting concrete with and without fibers. *Journal of Advanced Concrete Technology*, 11(10):251–265.

[13] Poppe, A. M., Schutter, G. D. (2005). Creep and shrinkage of self-compacting concrete. In *First International Symposium on Design, Performance and Use of Self-Consolidating Concrete*, Hunan, China, 329–336.

[14] Kavanaugh, B. P. (2008). Creep behavior of self-consolidating concrete. Master's thesis, Auburn University, Alabama.

[15] Huang, H. C. (2020). Regression of shrinkage and creep prediction formula of concrete in Taiwan based on database analysis and application on long-term deflection of prestressed concrete bridge. Master's thesis, National Taiwan University, Taipei, Taiwan (ROC). In Chinese.

[16] ASTM C150/C150M-19a (2019). *Standard specification for Portland cement*. West Conshohocken, PA: ASTM International.

[17] ASTM C618-19 (2019). *Standard specification for coal fly ash and raw or calcined natural pozzolan for use in concrete*. West Conshohocken, PA: ASTM International.

[18] ASTM C128-15 (2015). *Standard test method for relative density (specific gravity) and absorption of fine aggregate*. West Conshohocken, PA: ASTM International.

[19] ASTM C127-15 (2015). *Standard test method for relative density (specific gravity) and absorption of coarse aggregate*. West Conshohocken, PA: ASTM International.

[20] ASTM C1611/C1611M-18 (2018). *Standard test method for slump flow of self-consolidating concrete*. West Conshohocken, PA: ASTM International.

[21] EN 12350-9 (2010). *Testing fresh concrete - Part 9: Self-compacting concrete - V-funnel test*. Brussels, Belgium.

[22] ASTM C157/C157M-17 (2017). *Standard test method for length change of hardened hydraulic-cement mortar and concrete*. West Conshohocken, PA: ASTM International.
[23] ASTM C512/C512M-15 (2015). *Standard test method for creep of concrete in compression*. West Conshohocken, PA: ASTM International.
[24] ASTM C39/C39M-18 (2018). *Standard test method for compressive strength of cylindrical concrete specimens*. West Conshohocken, PA: ASTM International.
[25] European Project Group (2005). *The European guidelines for self-compacting concrete: Specification, production and use*. Brussels, Belgium.
[26] Lee, S. H., Kim, H. J., Sakai, E., Daimon, M. (2003). Effect of particle size distribution of fly ash-cement system on the fluidity of cement pastes. *Cement and Concrete Research*, 33(5):763–768.
[27] Khatib, J. (2008). Performance of self-compacting concrete containing fly ash. *Construction and Building Materials*, 22(9):1963–1971.
[28] Promsawat, P., Chatveera, B., Sua-iam, G., Makul, N. (2020). Properties of self-compacting concrete prepared with ternary Portland cement-high volume fly ash-calcium carbonate blends. *Case Studies in Construction Materials*, 13:e00426.
[29] Mustapha, F., Sulaiman, A., Mohamed, R., Umara, S. (2021). The effect of fly ash and silica fume on self-compacting high-performance concrete. *Materials Today: Proceedings*, 39(2):965–969.
[30] Pham, V.-N. (2025). Practical formulation for estimating the compressive strength of self-compacting fly ash concrete using gene-expression programming. *Journal of Science and Technology in Civil Engineering*, 19(3):98–109.
[31] Neville, A. M., Dilger, W. H., Brooks, J. J. (1983). *Creep of plain and structural concrete*. Construction Press, Essex.
[32] Jawahar, J. G., Sashidhar, C., Reddy, I. R., Peter, J. A. (2013). Micro and macrolevel properties of fly ash blended self compacting concrete. *Materials and Design*, 46(1):696–705.
[33] Mehta, P. K., Monteiro, P. J. M. (2006). *Concrete: Microstructure, properties, and materials*. McGraw Hill Education, New York.
[34] Nguyen, D. B., Liao, W. C. (2025). Optimization strategy of model B4TW-SCC in predicting shrinkage of self-compacting concrete. *Journal of Science and Technology in Civil Engineering*, 19(4):1–17.
[35] Montgomery, D. C., Peck, E. A., Vining, G. G. (2012). *Introduction to linear regression analysis*. John Wiley & Sons, New Jersey.
[36] Hami, A. E., Pougnet, P. (2020). *Embedded mechatronic systems 2: Analyses of failures, modeling, simulation and optimization*. ISTE Press and Elsevier, London.
[37] Dietterich, H. R., Lev, E., Chen, J., Richardson, J. A., Cashman, K. V. (2017). Benchmarking computational fluid dynamics models of lava flow simulation for hazard assessment, forecasting, and risk management. *Journal of Applied Volcanology*, 6(9):1–14.
[38] Rizi, F. S., Granitzer, M. (2017). Properties of vector embeddings in social networks. *Algorithms*, 10(4): 109.
[39] Wendner, R., Hubler, M. H., Bažant, Z. P. (2015). Optimization method, choice of form and uncertainty quantification of Model B4 using laboratory and multi-decade bridge databases. *Materials and Structures*, 48(4):771–796.
[40] Hubler, M. H., Wendner, R., Bažant, Z. P. (2015). Statistical justification of Model B4 for drying and autogenous shrinkage of concrete and comparisons to other models. *Materials and Structures*, 48(4): 797–814.